J Am Oil Chem Soc (2010) 87:1127–1136
DOI 10.1007/s11746-010-1601-2

ORIGINAL PAPER

Microscale Surface Roughening of Chocolate Viewed with Optical Profilometry

Dérick Rousseau · Sopark Sonwai · Rizwan Khan

Received: 17 September 2009 / Revised: 7 April 2010 / Accepted: 1 May 2010 / Published online: 27 June 2010

Abstract Microtopographical roughening and fat phase melting of milk chocolate subjected to three temperature cycles between 20 and 28, 30, 32, or 34 °C were examined using optical profilometry and differential scanning calorimetry (DSC). Cycling to any of these temperatures did not lead to immediate visual bloom, though significant effects on microstructure and fat phase melting behavior were noted. The initial chocolate topography was lightly mottled and consisted of small asperities. DSC indicated the presence of form V crystals in control chocolates kept isothermally, with form VI crystals appearing with cycling to 30 and 32 °C. The fat phase of the chocolates cycled to 34 °C existed only in the form IV polymorph. As a result of cycling, the surface roughness of all samples increased, with the smallest rise seen with cycling to 28 °C. Decomposition of the roughness into low and high-frequency components revealed a significant contribution of waviness (the low-frequency component) to overall roughness, particularly with cycling to 34 °C. Furthermore, with the fat phase fully molten, the backbone structure consisting of the dispersed particulates also contributed to overall roughness. This study demonstrated that significant microstructural changes and deformation take place within chocolate as a result of temperature fluctuations prior to the onset of visible surface fat bloom.

D. Rousseau (✉) · R. Khan
Department of Chemistry and Biology, Ryerson University,
350 Victoria Street, Toronto, ON M5B 2K3, Canada
e-mail: rousseau@ryerson.ca

S. Sonwai
Department of Food Technology,
Faculty of Engineering and Industrial Technology,
Silpakorn University, Nakornprathom 73000, Thailand

Keywords Chocolate · Optical profilometry · Cocoa butter · Melting · Roughness · Waviness

Introduction

Chocolate sensory properties such as snap, gloss, and melting profile strongly depend on the tempering and cooling of the fat phase as well as the subsequent storage conditions. Cocoa butter (CB), the key fat used in chocolate, is polymorphic and consists of six different crystalline forms (I through VI), with successive forms exhibiting increased thermodynamic stability [1, 2]. The polymorph in properly-crystallized chocolate is form V, and though not the most stable, confers the most desirable textural attributes.

Fat bloom is the unwanted, uncontrolled re-crystallization or polymorphic transition of CB form V crystals into form VI normally caused by the migration of lower-melting fats (e.g., in center-filled products) and/or temperature fluctuations during storage. In its mildest form, it appears as an overall dulling of the chocolate surface. In its extreme form, the appearance of the chocolate deteriorates significantly with the development of distinct white patches. This defect is primarily a surface phenomenon that results from crystals >5 μm in length that diffuse light, yielding a greyish, chalky appearance. Such topographical changes are also indicative of significant changes in the bulk properties of the chocolate.

Surface roughness, which is an indicator of fat bloom formation [3–5], can be ascertained with techniques such as atomic force microscopy (AFM), scanning electron microscopy, and laser scanning microscopy [6]. Optical profilometry (OP) has been used in many fields to characterize the micron-scale topography of materials (e.g.,

MEMS, films, dermatology, concrete, etc.) [7–10], yet no published results describe its use for the study of food texture and topography. This technique provides rapid surface analysis by utilizing light interferometry for high-resolution surface measurements [11]. Given that it is a non-contact technique, OP limits topographical deformation, which is appropriate when studying the early stages of structure development, e.g., liquid–solid transitions in lipid networks. In OP, white light is focused on a sample using an interferometric lens that moves vertically through the focal plane. The light reflected from the surface recombines with a reference beam and interference fringes are formed. The fringe pattern is captured on each pixel of a CCD camera array and referenced to the vertical position of the lens, with the accompanying software generating a 2D or 3D profile. As OP permits large scan sizes (e.g., ~3–4 mm^2), bigger surface features or periodicities are less likely to be overlooked than with AFM. However, OP performance somewhat depends on the reflectivity of the sample surface.

The topography of a material such as chocolate can be described by numerous textural parameters, namely roughness, waviness (upon which roughness is superimposed), surface anisotropy (i.e., the dominant direction or pattern in surface texture), atomic/molecular roughness, and unique errors (e.g., scratches, imperfections) [12, 13]. These frequently inter-related parameters exist at different length scales and usually provide insight regarding a material's bulk behavior. Based on preliminary analysis, neither surface anisotropy nor flaws were significant on the chocolates, and only roughness and waviness were evaluated as we were not interested in molecular-scale roughness.

In properly-tempered and stored chocolate, fat bloom can take months or years to set in. Temperature-cycling has been used to promote polymorphic transitions in crystal structures, often in pharmaceutical applications and to a lesser extent, in food products. With respect to chocolate, some groups have used this method to accelerate fat bloom onset and growth [3, 4, 14]. Here, we tailored the temperature gradients to take into account the distinct melting points of CB's key polymorphs, and determine how controlled re-crystallization and melting may significantly re-organize chocolate microstructure. The four setpoint temperatures (28, 30, 32, and 34 °C) were selected based on the melting points of the form IV, V, and VI CB polymorphs [15]. These were also based on previous reports where chocolate subjected to similar temperature gradients became distorted and difficult to characterize with AFM, given its limited z-axis range [4, 16].

The goals of this study were to: (1) establish a microstructural basis for the early stages of fat bloom development in milk chocolate prior to its visible onset and, (2) determine whether the microstructural changes catalyzed by temperature-cycling display a length-scale dependence.

Experimental Procedure

Milk chocolate bars (0.4 cm × 3 cm × 12 cm) were kindly provided by Cadbury Chocolates (Toronto, Canada). These crumb chocolates contained ~20% milk solids and ~30% fat, consisting of CB only. A Wyko NT1100 optical profiler (Veeco, Tucson, AZ, USA) was used to image 288 × 219 μm areas of the chocolate bar surface. To accelerate structural changes, the chocolates were cycled from 20 °C to setpoint temperatures of either 28, 30, 32, or 34 °C using a Peltier-controlled temperature stage (model TS62 with STC200 controller, Instec, Boulder, CO, USA) placed atop the optical profilometer stage. The concordance of the Peltier stage and chocolate surface temperatures was ascertained using a calibrated wire thermocouple mated to a digital thermometer. Slight discrepancies were observed, with the chocolate surface consistently 0.5 °C below a given setpoint. Thus, during OP analysis, the Peltier stage was adjusted to attain the desired endpoint temperature on the chocolate.

For each cycle, individual samples were heated from 20 °C to a given setpoint at 5 °C/min where they were held for 1 h before being brought back to 20 °C at 5 °C/min and held for 1 h (Fig. 1). Samples were subjected to three cycles, with OP characterization taking place during the last 5 min of each cycle at 20 °C. These samples were then stored at room temperature (~25 °C) to assess whether cycling led to visual bloom. At least ten different chocolate bars were cycled to each setpoint temperature. Control samples were stored at room temperature for the same duration as the samples subjected to cycling. To obtain

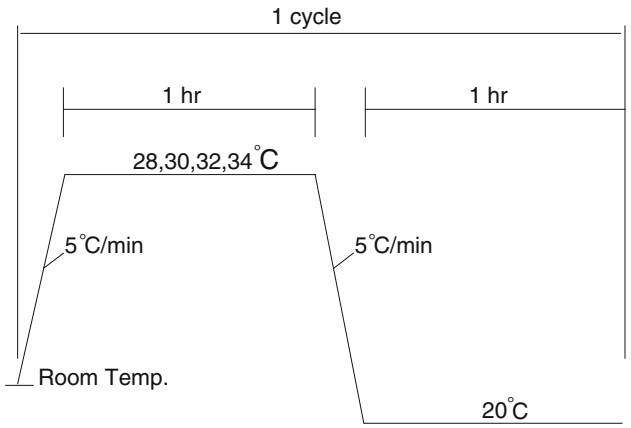

Fig. 1 Temperature protocol used to cycle the milk chocolate samples. Samples were cycled between 20 and either 28, 30, 32, or 34 °C for up to three cycles. Each experiment lasted ~6 h

representative roughness measurements, randomly-located measurements were carried out on each sample. Where necessary, a digital correction of the topography images was performed with the OP software due to localized absence of height data, given the inherently low reflectivity of the chocolate surface and/or steep angle between adjacent data points. Missing data points were approximated using a smooth shape calculated from nearest neighbor distances. Images shown are representative of the microstructure seen after a given cycle and setpoint temperature.

It is important to characterize the texture of a surface, with roughness a commonly-used parameter. Overall roughness was reported as *Rq* and calculated as follows:

$$Rq = \sqrt{\frac{1}{N}\sum_{i=1}^{N} Z_i^2} \quad (1)$$

where Z and N are the individual height deviations from the mean data plane and the number of measurements, respectively. The descriptor *Rq* may be replaced by *Wq* (waviness) following spectral decomposition. These descriptors, though very popular, do not always accurately reflect surface properties, as neither the distance between features nor surface anisotropy are determined [17]. Nevertheless, for the purpose of identifying whether microstructural changes took place at different length scales, this approach was deemed appropriate. As *Rq* and *Wq* values inherently depend on the size of the area measured, all images were captured with fields of view of 219 × 288 μm, which allowed for direct sample comparison. To distinguish *Rq* from *Wq*, the chocolate topographical profiles were filtered and decomposed into two images above and below a spatial frequency of 25/mm using a Fast Fourier Transform algorithm. Although ISO has introduced specified filter cutoff lengths of 8, 2.5, 0.8, 0.25, and 0.08 mm [18], a value of 0.04 mm was used as it permitted isolation of the contribution of surface waviness to overall (unfiltered) roughness.

The distribution of surface heights after each cycle and at each setpoint was evaluated with histograms, with the height data grouped into 200 bins as per the initial image capture. Descriptive statistics [skewness (Sk) and kurtosis (Ku)] were evaluated using Easyfit 5.0 Professional software (Mathwave Technologies, Spokane, WA, USA). The goodness of fit between the measured height distributions and a Gaussian distribution was determined using the Kolmogorov–Smirnov test [19].

A Perkin Elmer Pyris Diamond differential scanning calorimeter (DSC) (Perkin-Elmer, Woodbridge, ON, Canada) was used to characterize the temperature-cycled chocolates' fat phase melting behavior. Scans from 20 to 60 °C at 5 °C/min were performed following three in situ cycles to each setpoint temperature using the protocol mentioned earlier. The instrument was calibrated using a traceable indium reference standard (m.p. = 156.6 °C and H_f = 28.71 J/g).

All results are presented as means ± SDs, and were graphed and statistically analyzed with SigmaPlot software (version 11.0, Systat Inc., Chicago, IL). Between-group differences in unfiltered (overall) roughness as well as filtered roughness and waviness values were analyzed with one-way ANOVAs and the Holm-Sidak post hoc test. The level of significance was set at $p < 0.05$.

Results and Discussion

Control Chocolate Topography

Prior to temperature-cycling, the landscape of the fresh chocolates was smooth and free of any surface dulling, with OP images revealing the presence of small, evenly-distributed asperities (Fig. 2). Overall *Rq* roughnesses for all controls (170–218 nm) were statistically significantly different from each other ($p < 0.05$) (Table 1), except for the 20–28 and 20–34 °C ($p > 0.05$). These unexpected results were due to the small within-group *Rq* differences (low coefficients of variation, CV) and variability present between the initial chocolate themselves (Table 1). These roughness values were similar to AFM-based

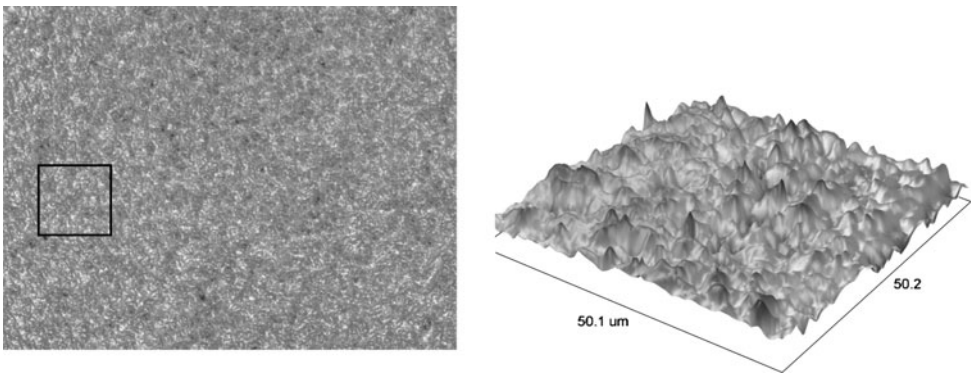

Fig. 2 Surface of freshly-made ('control') chocolate imaged with optical profilometry. *Left-hand* image is 219 × 288 μm with a *z*-axis scale of 5 μm. *Right-hand* image is a 50 × 50 μm close-up with a 2 μm *z*-axis scale (*black square*)

Table 1 Evolution in unfiltered *Rq* surface roughness as a function of number of cycles and temperature regime used, along with associated coefficients of variation (CV) in %

Regime	0 cycle	CV (%)	1 cycle	CV (%)	2 cycles	CV (%)	3 cycles	CV (%)
20–28 °C	218.3 ± 11.2	5.1	361.4 ± 16.3	4.5	402.7 ± 20.2	5.0	442.9 ± 24.8	5.6
20–30 °C	170.0 ± 9.4	5.5	370.6 ± 31.8	8.6	404.5 ± 33.9	8.4	475.4 ± 72.4	15.2
20–32 °C	187.2 ± 7.3	3.9	437.7 ± 30.7	7.0	440.1 ± 32.5	7.4	515.3 ± 96.8	18.8
20–34 °C	215.6 ± 17.6	8.2	395.6 ± 10.3	2.6	538.5 ± 47.8	8.9	634.9 ± 35.9	5.7

measurements for fresh chocolate (~150–170 nm) [20]. All control chocolate images ($N = 40$) were generally devoid of surface depressions deeper than 1.5 μm. However, there existed infrequent depressions deeper than 3 μm that may have indicated some surface porosity.

Cycling-Induced Changes in Topography and Unfiltered Roughness

Visual appreciation of the OP images indicated that there was no preferential orientation to the topographical features on any of the chocolates. The surface of the chocolate cycled between 20 and 28 °C was smooth and free of any visible dulling or bloom throughout the study. However, the use of OP revealed notable changes in microtopography, with the gradual emergence of surface irregularities after 1, 2, and 3 cycles (Fig. 3). Crystal growth was apparent after two cycles (*black arrow*) whereas sizeable surface depressions appeared after three cycles. For example, the region shown by the white arrow was 4.8 μm deep and ~15 μm by ~10 μm in size. Unfiltered surface *Rq* doubled after three cycles (Table 1) from 218 to 442 nm, with changes in surface roughness statistically significantly different from one another after 1, 2, and 3 cycles ($p < 0.05$). In the chocolate cycled to 30 °C, the surface coarsened more extensively, as *Rq* values increased from 170 to 475 nm over three cycles (Fig. 4). Changes in surface roughness were also statistically significantly different after 1, 2, and 3 cycles ($p < 0.05$). Also visible were grouped surface depressions (*white circles*) indicative of region-dependent structural changes taking place as a result of repeated melting and crystallization. Cycling between 20 and 32 °C led to major microstructural changes (Fig. 5), with OP images showing dramatic microscale surface undulations. However, the increase in overall roughness was similar to that observed with cycling to 30 °C, clearly indicating that parameter *Rq* did not accurately reflect changes in topography [17]. Finally, the chocolate cycled to 34 °C showed the greatest changes in microtopography (Fig. 6), as *Rq* values nearly tripled after 3 cycles from 215 to 634 nm. Surface roughness after one cycle at 34 °C was similar to that observed after two cycles to 28 °C. Undulations indicative of bulk microstructural rearrangement were apparent after 1, 2, and 3 cycles, and suggested that the fat crystal network encasing the dispersed particulates was melting and recrystallizing in an uncontrolled manner. These results supported the concept of compositional heterogeneity playing a role in fat phase microstructural evolution, as some regions were more susceptible to deformation than others. The chocolates cycled to 32 and 34 °C and subsequently stored at room temperature eventually displayed visual bloom within 2 weeks.

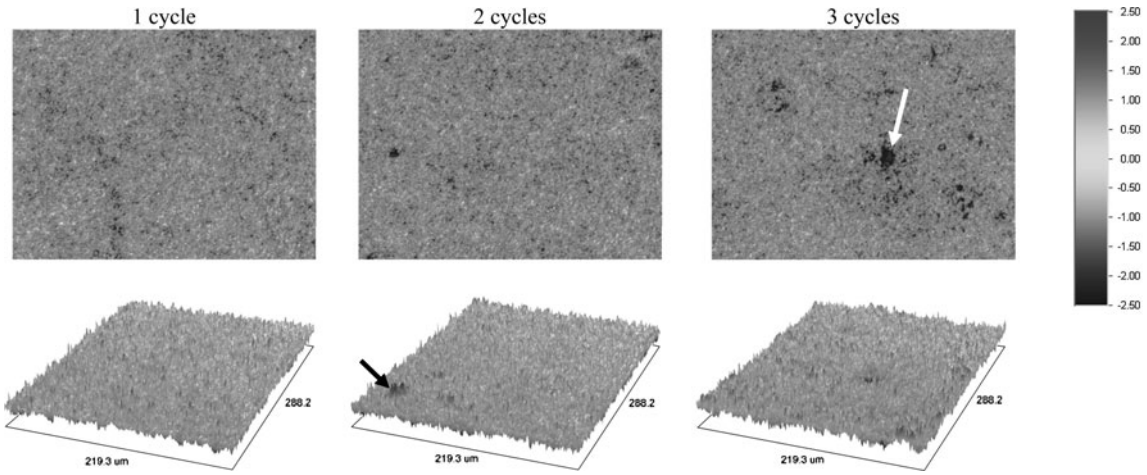

Fig. 3 Effect of temperature cycling between 20 and 28 °C. The *top row* represents 2D views after 1, 2, and 3 cycles, with the *lower row* showing corresponding 3D views. Images are 219 × 288 μm with a 5-μm *z*-axis scale (−2.5 to +2.5 μm)

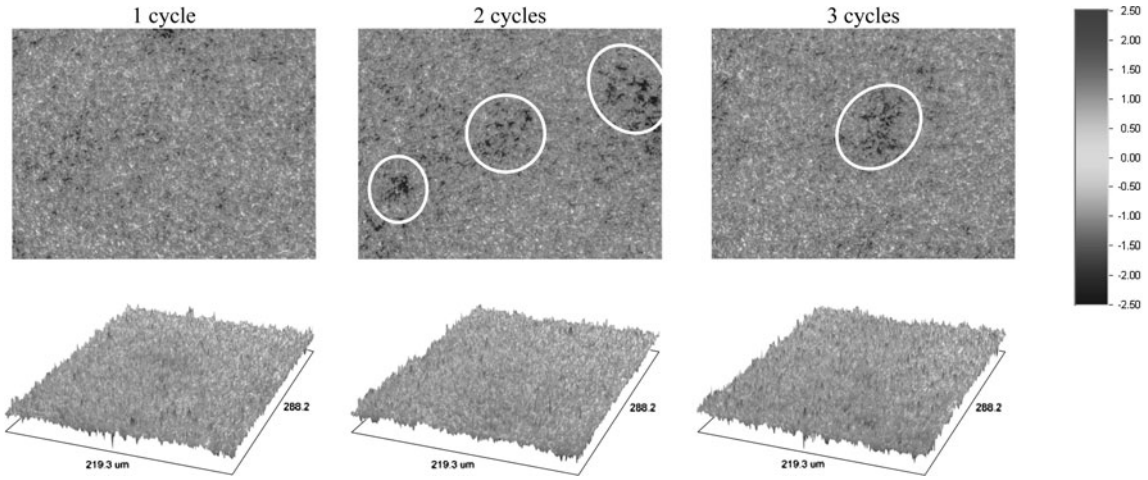

Fig. 4 Effect of temperature cycling between 20 and 30 °C. The *top row* represents 2D views after 1, 2, and 3 cycles, with the *lower row* showing corresponding 3D views. Images are 219 × 288 μm with a 5-μm *z*-axis scale (−2.5 to +2.5 μm)

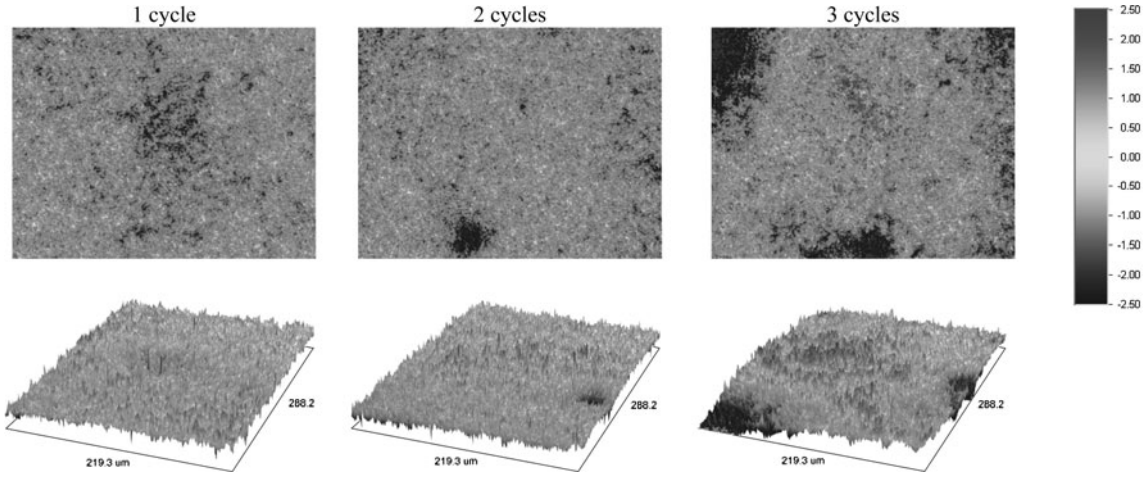

Fig. 5 Effect of temperature cycling between 20 and 32 °C. The *top row* represents 2D views after 1, 2, and 3 cycles, with the *lower row* showing corresponding 3D views. Images are 219 × 288 μm with a 5-μm *z*-axis scale (−2.5 to +2.5 μm)

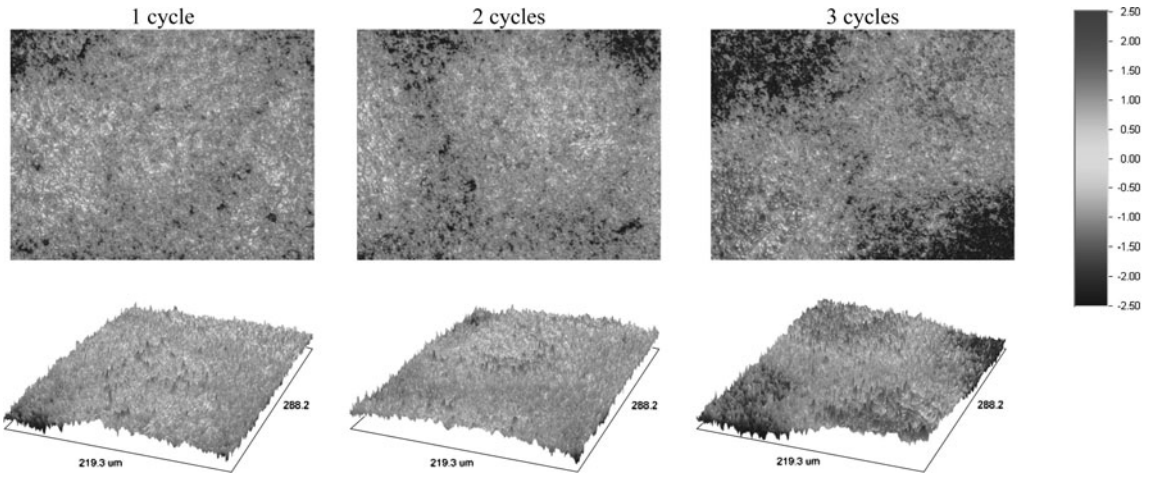

Fig. 6 Effect of temperature cycling between 20 and 34 °C. The *top row* represents 2D views after 1, 2, and 3 cycles, with the *lower row* showing corresponding 3D views. Images are 219 × 288 μm with a 5-μm *z*-axis scale (−2.5 to +2.5 μm)

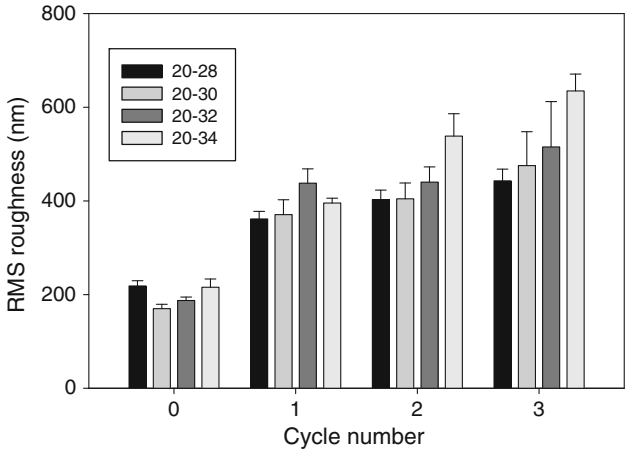

Fig. 7 Evolution in surface roughness as a function of temperature-cycling ($n \geq 10$)

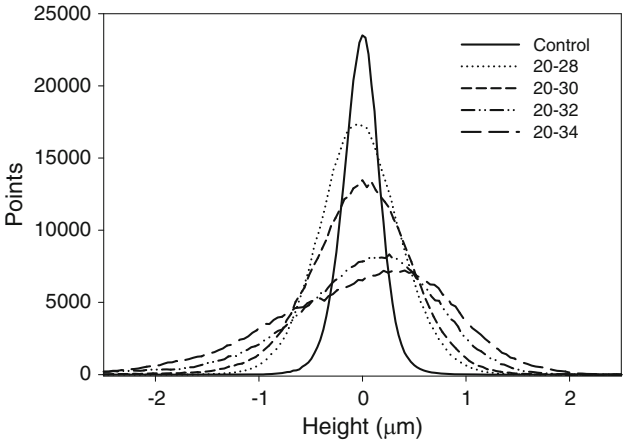

Fig. 8 Histogram showing the number of data points at each surface height following three temperature cycles with setpoint temperatures of 28, 30, 32, or 34 °C

The evolution in unfiltered *Rq* values demonstrated that the number of cycles and higher setpoint temperatures led to statistically significantly different roughnesses (Fig. 7; Table 2). Comparison of 20–34 °C versus 20–32, 20–30, and 20–28 °C confirmed significant unfiltered *Rq* differences after 1, 2, and 3 cycles ($p < 0.05$). However, no significant differences existed between setpoint temperatures of 28 or 30 °C (20–28 vs. 20–30 °C) after 1, 2, or 3 cycles ($p > 0.05$). Comparison of *Rq* values after three cycles with setpoint temperatures of 30 or 32 °C (20–30 vs. 20–32 °C) also showed no significant differences ($p > 0.05$). Overall, these results showed that larger temperature gradients lead to statistically significant changes in overall roughness.

Figure 8 combines representative histograms of the surface feature height distributions following 3 cycles to either 28, 30, 32, or 34 °C compared to that of a control chocolate. All height distributions were normally-distributed, based on the Kolmogorov–Smirnov goodness of fit test. With cycling to higher temperatures, the distributions widened and flattened, and generally demonstrated some kurtosis (Ku) and/or skewness (Sk). On the control, 95% of the asperities lay between −0.41 and 0.35 μm from the midpoint. A Ku = 1.48 and Sk near zero (−0.14) also characterized this distribution, and suggested great uniformity of surface features, with few valleys or jutting crystals. With cycling, there was an increase in the breadth of height points, particularly with larger temperature gradients. As a result of cycling to 28 °C, 95% of all surface features were between −0.85 and 0.70 μm, along with slight kurtosis (Ku = 0.4) and little skewness (Sk = 0.04). On the 20–30 °C chocolate, 95% of height data were between −1.03 and 0.86 μm, with a Ku of 1.44 and more evident skewness (Sk = −0.44). Through cycling to 32 °C, 95% of features were between −1.48 and 1.26 μm, with significant kurtosis (Ku = 1.41) and skewness (Sk = −0.80). Finally, with the 20–34 °C regime, 95% of surface heights were between −1.84 and 1.39 μm. Kurtosis of the distribution was no longer evident (Ku = 0.04), though some skewness was apparent (−0.44). As well, there was a slight tendency towards bimodality in this distribution, which was likely related to the extensive melting of the fat phase and its subsequent uncontrolled resolidification. The longer left tail of the height distributions with cycling to 30, 32, or 34 °C suggested that significant microstructural rearrangement had taken place. By contrast, the control and 20–28 °C height distributions were symmetric about the midpoint.

Table 2 Pairwise comparison of the effect of endpoint temperature and cycle on chocolate surface roughness (*Rq*) using the Holm-Sidak method

Comparison	0 cycle	1 cycle	2 cycles	3 cycles
20–28 versus 20–30 °C	<0.001	0.399	0.910	0.266
20–28 versus 20–32 °C	<0.001	<0.001	0.022	0.016
20–28 versus 20–34 °C	0.652	0.003	<0.001	<0.001
20–30 versus 20–32 °C	0.002	<0.001	0.029	0.174
20–30 versus 20–34 °C	<0.001	0.026	<0.001	<0.001
20–32 versus 20–34 °C	<0.001	<0.001	<0.001	<0.001

The level of significance was set at $p < 0.05$

Spectral Decomposition of Overall Roughness

Chocolate topography may be considered to be a global function that can be divided into components of different frequencies, with the surface a Fourier series with components originating from *Rq* and *Wq*. In this context, roughness was redefined as a characteristic of the chocolate surface accounting for irregularities associated with the

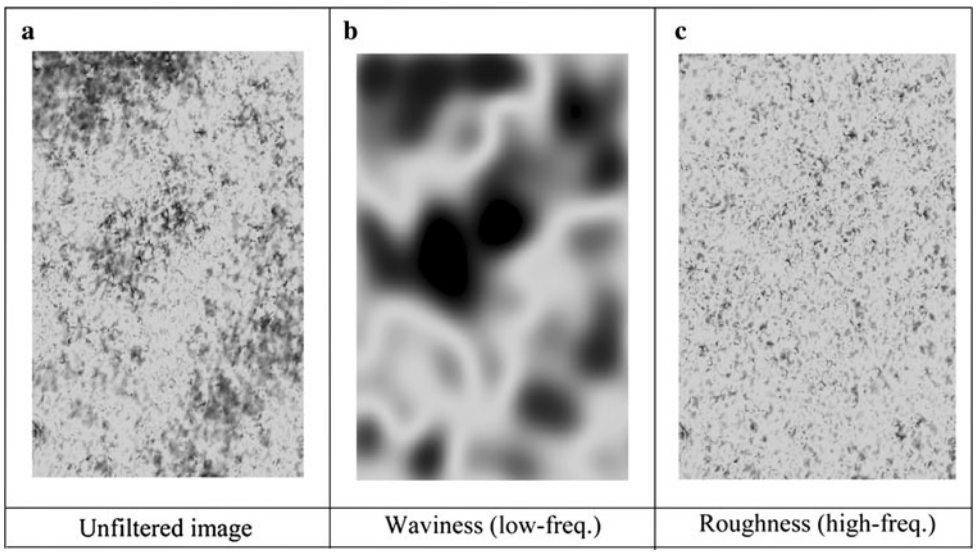

Fig. 9 Surface spectral decomposition of chocolate cycled three times between 20 and 34 °C **a** shows the unfiltered surface image; **b** shows the waviness (low-frequency) component, whereas **c** shows the roughness (high-frequency) component

growth of individual fat crystals and *Wq* was redefined as a measure of widely-spaced irregularities associated with "background" fat crystal network microstructural undulations. Figure 9a shows the unfiltered surface profile of chocolate cycled three times between 20 and 34 °C. Figure 9b, c show the decomposed height profile of this surface where *Wq* and *Rq* have been extracted. Together, these two images represent the 'sum' of the chocolate's topography.

In delineating the contributions of *Rq* and *Wq* to the surface profiles, care was taken to specify a meaningful cutoff filtering length (CFL). Though not typical of ISO CFLs [18], with a CFL of 0.04 mm, no statistically significantly differences in filtered *Rq* roughnesses after 2 and 3 cycles at all temperature setpoints existed ($p > 0.05$). Although it can be argued that selecting a CFL where the filtered *Rq* values are no longer statistically significantly different artificially forces the distribution towards larger *Wq* values, the purpose of this spectral decomposition was very much to ascertain whether *Wq* can contribute to the microtopographical changes seen in chocolate.

Figure 10 compares the evolution in the decomposed *Rq* and *Wq* values as a function of temperature setpoint and number of cycles. Based on the selected CFL, there was little change in filtered roughness with temperature cycling, as *Rq* values generally increased from ~200 to ~400 nm after three cycles at each setpoint. However, statistically significantly different *Wq* values existed after 2 and 3 cycles, with higher setpoint temperatures leading to gradually higher *Wq* values ($p < 0.05$). After two cycles, *Wq* increased from ~100 nm at 28 °C to ~330 nm at 34 °C whereas after three cycles, *Wq* increased from ~121 to ~450 nm at these temperatures. These results signified that with larger temperature gradients, *Wq* was contributing to chocolate roughness to a greater extent, with the role of individual fat crystals not dominating the observed *Rq* increase.

Bulk Fat Phase Melting and Thermal Deformation

Based on DSC-measured melting points, fresh chocolate was predominantly in the form V polymorph with a slight amount of form IV. Results showed that the form IV and V polymorphs melted at 27–29 °C and ~31–32 °C, respectively [21, 22]. Armed with these results, the temperature-cycling protocol was based on temperatures that represented these strategic transitions. A setpoint of 28 °C was selected as form IV would at least be partially melted,

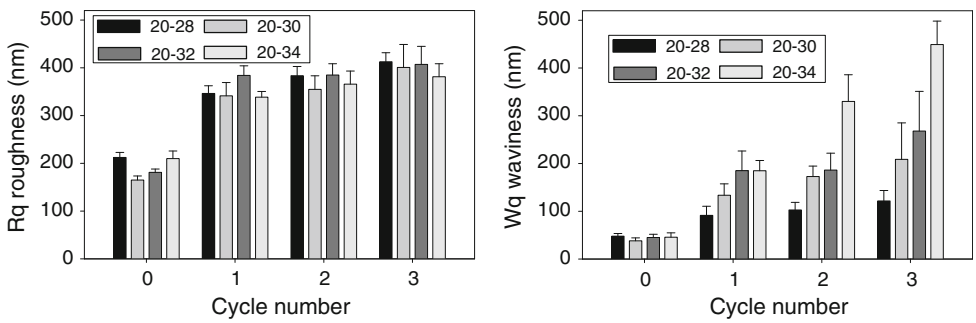

Fig. 10 Evolution in roughness and waviness of temperature-cycled chocolates following spectral decomposition ($n \geq 10$)

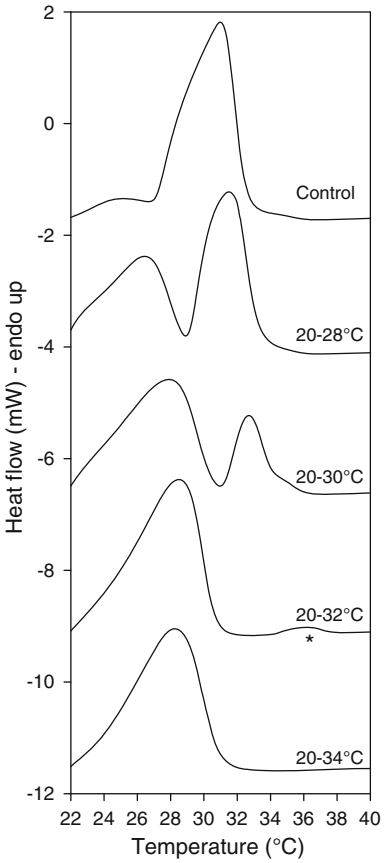

Fig. 11 Fat phase melting of chocolates temperature-cycled three times between 20 and 28, 30, 32, or 34 °C measured with DSC

while at 30 °C, it would fully melt with only limited melting of form V crystals. A temperature of 32 °C was expected to melt form V crystals whereas cycling to 34 °C would lead to full fat phase liquefaction.

Figure 11 compares the DSC fat phase melting profiles of the chocolates cycled 3 times to 28, 30, 32, or 34 °C. The control chocolate consisted of a single melting peak at 31 °C, presumably associated with form V crystals. A shoulder at ~29 °C was visible, indicative of a small amount of form IV crystals that originated from the crystallization of molten fat cooled to 20 °C during the DSC protocol (the fat phase of the fresh chocolates did consist of ~20% liquid fat, based on solid fat content results at 25 °C, results not shown). With three cycles to 28 °C, two distinct exotherms were visible, with peak temperatures of ~26.6 and ~31.6 °C corresponding to form IV and V CB polymorphs. These results suggested that cycling to 28 °C led to partial melting of the fat phase and its recrystallization into form IV, with no form VI crystal formation. After three cycles to 30 °C, two exotherms at ~27.9 and ~32.8 °C corresponding to form IV and V CB polymorphs were visible. Smaller form V crystals that melted by 30 °C recrystallized into form IV, which resulted in a larger form IV peak. A small shoulder to the right of the 32.8 °C peak at ~35 °C suggested the possibility of a small proportion of form VI crystals. With cycling to 32 °C, the form V peak completely disappeared and a distinct form VI peak appeared at 36.2 °C (shown with an asterisk). Most of the fat phase thus melted and recrystallized into form IV (peak at 28.5 °C). With cycling to 34 °C, only form IV crystals were visible, suggesting complete melting of the chocolate fat phase and no transition towards either forms V or VI.

There is a clear link between the change in bulk fat phase melting behavior and the microtopographical changes seen. Larger temperature gradients led to statistically significant changes in unfiltered roughness ($p < 0.05$), and the increased contribution of *Wq* over filtered *Rq* to overall roughness. DSC results confirmed that progressively higher temperature setpoints resulted in accrued melting of the fat phase. Though it may be presumed that the increase in unfiltered roughness was due to uncontrolled CB re-crystallization or the form V→VI transition, spectral decomposition demonstrated that there was little difference in *Rq* roughness as a function of setpoint temperature. Thus, topographical changes were not driven by the re-crystallization and growth of individual surface crystals, but rather by bulk fat crystal network-driven microstructural changes that led to higher *Wq* values. Having the initial form V crystals generated through proper tempering melt and uncontrollably recrystallize as form IV crystals (and to a lesser extent, as form VI) resulted in 'warping' and higher *Wq* values at higher temperature setpoints. In the absence of a polymorphic transition at lower setpoints, there was perhaps an increase in the average crystal size due to the temperature-cycling or perhaps Ostwald ripening that may have contributed to the undulations seen. However, as each temperature cycle was short (~2 h), crystallization kinetics were such that newly-formed CB crystals would not have sufficient time to grow and dominate the changes seen in roughness.

To further delineate how the evolution in fat phase microstructure was contributing to surface roughness, chocolates subjected to three cycles from 20–34 °C were heated to 45 °C (and held 1 h) and subsequently cooled to 15 °C (and held for 1 h). Changes in topography from this thermal treatment were readily apparent (Fig. 12). Figure 12a shows the surface structure of chocolate where the fat phase is fully molten (45 °C). Though little surface structure would be expected given the liquefied fat phase, the unfiltered *Rq* value of this surface was ~340 nm—a value similar to one 20–34 °C cycle. Furthermore, the corresponding cross-sectional profile (Fig. 12b) clearly shows that substantial topographical features remained. In theory, such microstructure can only correspond to the non-fat components present in the milk chocolate (milk powder, cocoa solids, and sugar) which form a concrete-like

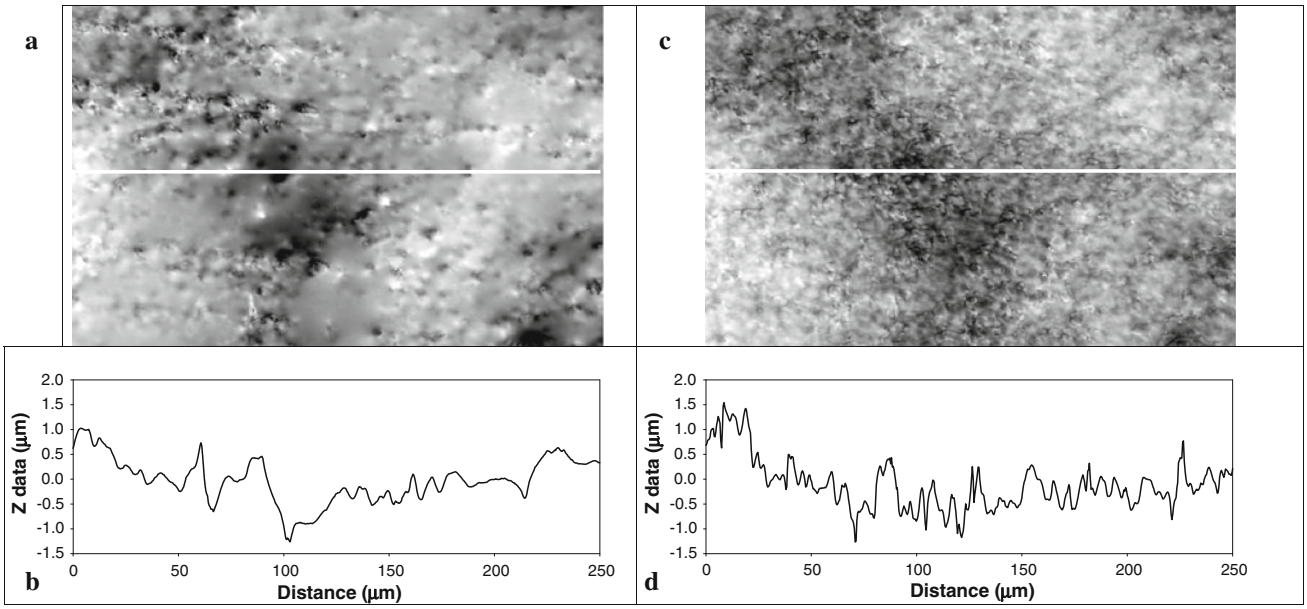

Fig. 12 Surface of chocolate at 45 °C (fully molten fat phase) (**a**) and 15 °C (solidified fat phase) (**c**). The cross-sectional profile in (**b**) corresponds to the *white line* shown in (**a**) whereas (**d**) corresponds to the *white line* shown in (**c**)

backbone network presumably held in place by various interactions (electrostatic, capillary, etc.). Solidification of this same region to 15 °C (Fig. 12c) revealed a significantly different surface texture, one associated with extensive fat phase crystallization, as per the cross-sectional profile (Fig. 12d) (unfiltered Rq, ~490 nm). Jaggedness is evidence of crystal growth, which is superimposed onto the particulate network roughness seen in Fig. 12a. These results clearly demonstrated that the fat phase was not the sole contributor to surface texture, and that the particulate network also played a role in topographical changes and overall roughness.

Conclusions

Significant microstructural changes take place in milk chocolate prior to the onset of visible surface fat bloom. As a result of temperature-cycling, a length-scale dependence on the structural rearrangement exists, with lower-frequency features (waviness) becoming dominant as the chocolate is subjected to higher temperature setpoints. Notably, cycling temperatures close to or above the form V melting point result in considerable bulk deformation of the fat crystal network which is seen as 'background' undulations. Such buckling may be an important factor in the initiation and development of fat bloom in chocolate.

Secondly, using OP to monitor the topography of chocolate has proven a viable alternative to other instruments such as AFM in detecting changes in the surface morphology of chocolate. This technique is capable of visualizing a much larger area in a much shorter amount of time, albeit with a loss in resolution. Overall, it is promising as a tool for studying more of the causative factors in chocolate fat bloom under various scenarios of inducement.

Acknowledgments Funding from the Natural Sciences and Engineering Research Council (NSERC) of Canada is acknowledged. Mr. Nigel Sanders from Cadbury Canada (Toronto) is thanked for making and supplying chocolates. Mr. Shane Hodge is thanked for his assistance with experiments.

References

1. Wille RL, Lutton ES (1966) Polymorphism of cocoa butter. J Am Oil Chem Soc 43:491–496
2. deMan JM (1992) X-ray diffraction spectroscopy in the study of fat polymorphism. Food Res Int 25:471–476
3. Bricknell J, Hartel RW (1998) Relation of fat bloom in chocolate to polymorphic transitions of cocoa butter. J Am Oil Chem Soc 75:1609–1615
4. Hodge SM, Rousseau D (2002) Fat bloom formation and characterization in milk chocolate observed by atomic force microscopy. J Am Oil Chem Soc 79:1115–1121
5. Quevedo R, Brown C, Bouchon P, Aguilera JM (2005) Surface roughness during storage of chocolate: fractal analysis and possible mechanisms. J Am Oil Chem Soc 82:457–462
6. Briones V, Aguilera JM, Brown C (2006) Effect of surface topography on color and gloss of chocolate. J Food Eng 77:776–783
7. Garbacz A, Courard L, Katarzyna K (2006) Characterization of concrete surface roughness and its relation to adhesion in repair systems. Mater Charact 56:281–289
8. Waits CM, Morgan B, Kastantin M, Ghodssi R (2005) Microfabrication of 3D silicon MEMS structures using gray-scale lithography and deep reactive ion etching. Sens Actuators A Phys 119:245–253

9. Smallen M, Lee JJK (1993) Pole tip recession measurements on thin film heads using optical profilometry with phase correction and atomic force microscopy. J Tribol 115:382–387
10. Grove GL, Grove MJ, Leyden JJ (1989) Optical profilometry: an objective method for quantification of facial wrinkles. J Am Acad Dermatol 21:631–637
11. Wyant JC, Koliopoulos CL, Bhushan B, George OE (1984) An optical profilometer for surface characterization of magnetic media. ASLE Trans 27:101–113
12. Myshkin NK, Grigoriev A, Chizhik SA, Choi KY, Petrokovets MI (2003) Surface roughness and texture analysis in microscale. Wear 254:1001–1009
13. Howell D, Behrends B (2006) A review of surface roughness in antifouling coatings illustrating the importance of cutoff length. Biofouling 22:401–410
14. Hachiya I, Koyano T, Sato K (1989) Seeding effects on solidification behaviour of cocoa butter and dark chocolate II. Physical properties of dark chocolate. J Am Oil Chem Soc 66:1763–1770
15. Loisel C, Keller G, Lecq G, Bourgaux C, Ollivon M (1998) Phase transitions and polymorphism of cocoa butter. J Am Oil Chem Soc 75:425–439
16. Rousseau D (2006) On the porous mesostructure of milk chocolate viewed with atomic force microscopy. Lebensm Wiss Technol 39:852–860
17. Assender H, Bliznyuk V, Porfyrakis K (2002) How surface topography relates to materials' properties. Science 297:973–976
18. ISO (1998) ISO 4288:1996/Cor 1:1998. Geometrical product specifications (GPS)—surface texture: profile method—rules and procedures for the assessment of surface texture. Report No BS 3900-K2:2001. International Standards Organization, London
19. Chakravarti IM, Laha RG, Roy J (1967) Handbook of methods of applied statistics, vol I. Wiley, New York
20. Sonwai S, Rousseau D (2010) Controlling fat bloom formation in chocolate—impact of milk fat on microstructure and fat phase crystallization. Food Chem 119:286–297
21. Timms RE (2003) Confectionery fats handbook—properties production and application. Oily Press, Dundee
22. Beckett ST (2000) The science of chocolate. The Royal Society of Chemistry. Cambridge, UK